Electronic Supplementary Material (ESI) for RSC Advances.

Supplementary Information

Theoretical Evaluation of the Structure-Activity Relationship in Graphene-based Electrocatalysts for a Hydrogen Evolution Reactions

*Chi Ho Lee[1], Byoengsun Jun[1] and Sang Uck Lee[1,2]**

[1]Department of Bionano Technology, Hanyang University, Ansan 15588, Korea.

[2]Department of Chemical & Molecular Engineering, Hanyang University, Ansan 15588, Korea.

* Corresponding author. Email: sulee@hanyang.ac.kr

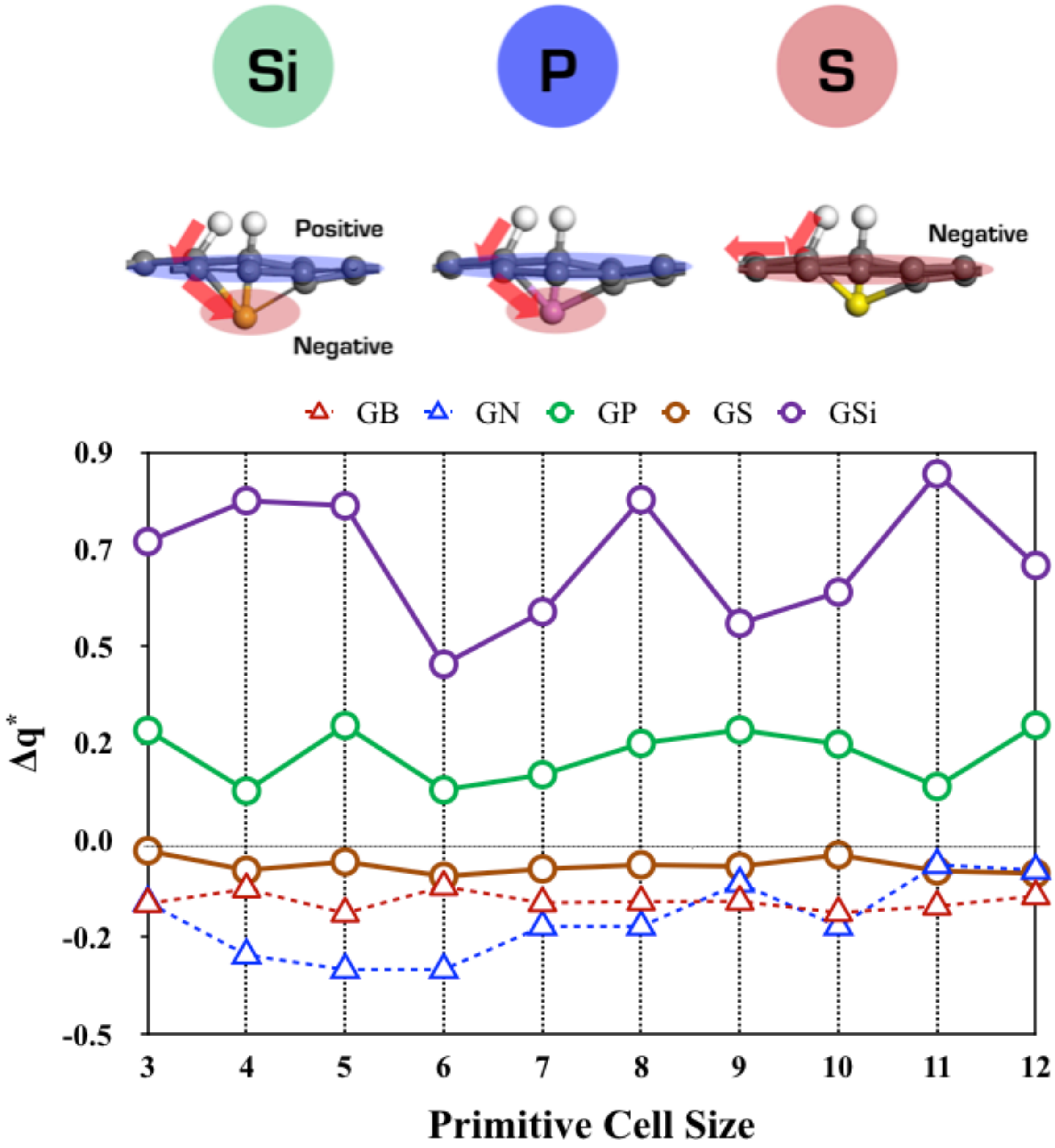

Figure S1. Variation of charge around active sites by hydrogen binding. q* indicates charge of carbons around active sites. $\Delta q^* = q^*_{GX+2H} - q^*_{GX}$

HER activity depends on the stability of the adsorbed hydrogen atoms on the surface of the catalyst as the intermediate state (H*). Because the hydrogen adsorption (Volmer step) is endothermic, enhanced hydrogen binding can improve HER activity. First of all, the stability of the intermediate state (H*) is determined by the type of hybridization of active site carbon; sp^3 hybridized carbons in out-of-plane structures (GS, GP and GSi) more readily form a hydrogen atom binding rather than sp^2 in in-plane structures (GB and GN). Then, in the same out-of-plane structures, the hydrogen atom binding energy depends on the charge of the carbons around the active site with ionic bond characters. Therefore, the negativity of carbon charges around active sites by hydrogen binding improve HER activity. Looking at the Figure S4, the order of negativity of carbon charges around active site is well agreement with the order of HER activity. The less negativity of carbon charges on GSi and GP can be explained by charge localization on the dopant as shown in Figure S4.

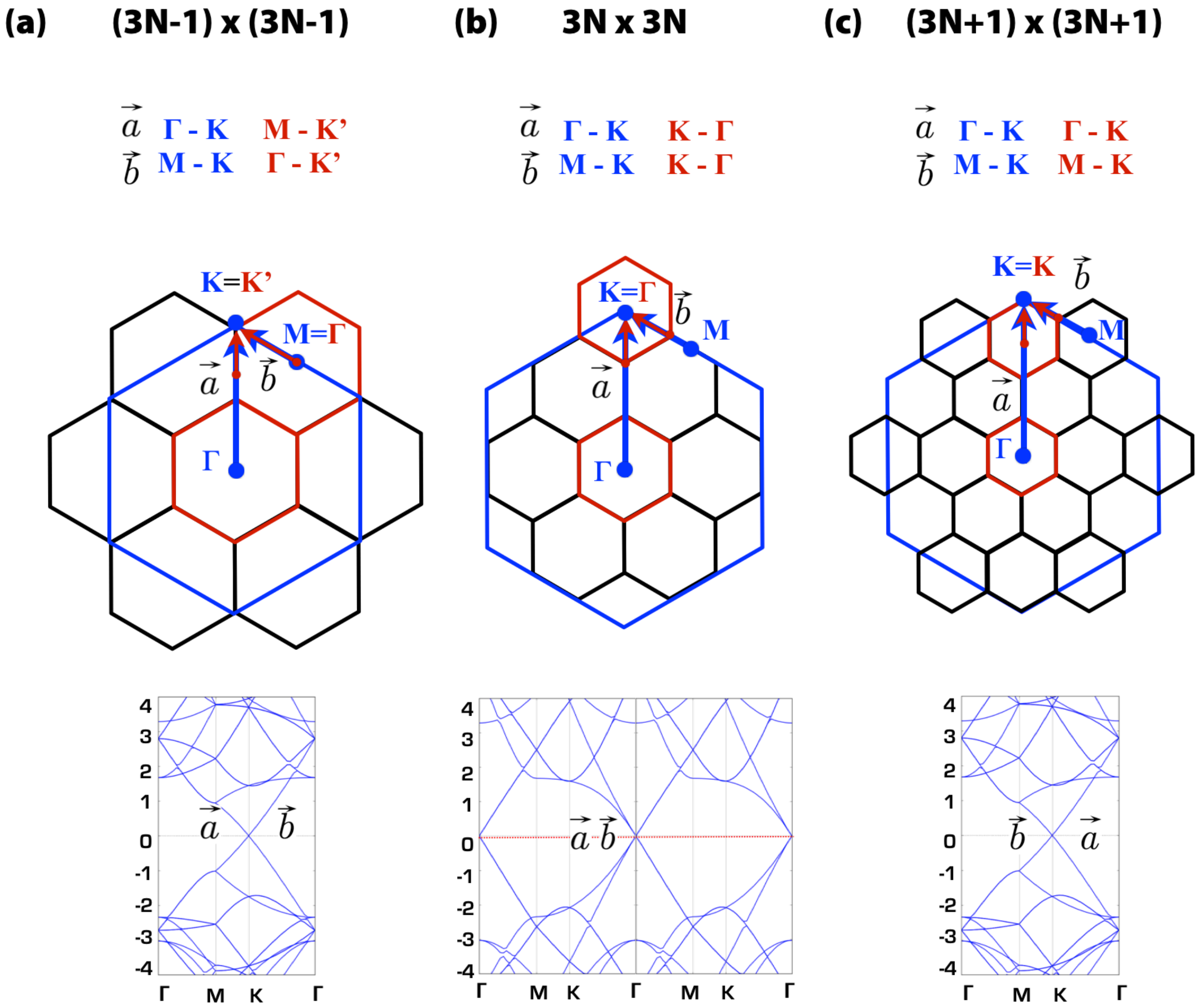

Figure S2. The first Brillouin zone of (a) (3N-1) x (3N-1), (b) 3N x 3N, and (c) (3N+1) x (3N+1) supercells with band structures. The blue lines represent the first Brillouin zone of the primitive cell. The black and red lines are the first Brillouin zones of the supercells. The blue and red arrows are k-path around Dirac point of primitive cell and super cell, respectively. $\vec{\boldsymbol{a}}$ and $\vec{\boldsymbol{b}}$ indicate Γ−K and M−K path at primitive cell.

The 3N rule can be explained by band folding as shown in Figure S1. The energy band diagram is normally plotted within the first Brillouin zone. Any wavevector in the higher Brillouin zones can be folded into its corresponding wavevector in the first Brillouin zone. For a $3N \times 3N$ supercell, the Dirac points are moved to the Γ point via the translational symmetry operation, hence the Dirac points are folded to the Γ points instead of K points and which produces two bands near the Γ points because Γ−K and M−K paths are degenerated to Γ−K as shown in Figure 2S (b). Therefore, $\vec{\boldsymbol{a}}$ and $\vec{\boldsymbol{b}}$ paths are equivalent. While, for the $(3N-1) \times (3N-1)$ supercells, the Dirac points are folded to the K and K' points and $\vec{\boldsymbol{a}}$ and $\vec{\boldsymbol{b}}$ paths are exchanged. For the $(3N+1) \times (3N+1)$ supercells, the Dirac points are always folded to the K point and there is no change in $\vec{\boldsymbol{a}}$ and $\vec{\boldsymbol{b}}$ paths. Consequently, the notable $3N \times 3N$ band structure produces distinct electronic properties as well as HER activity.

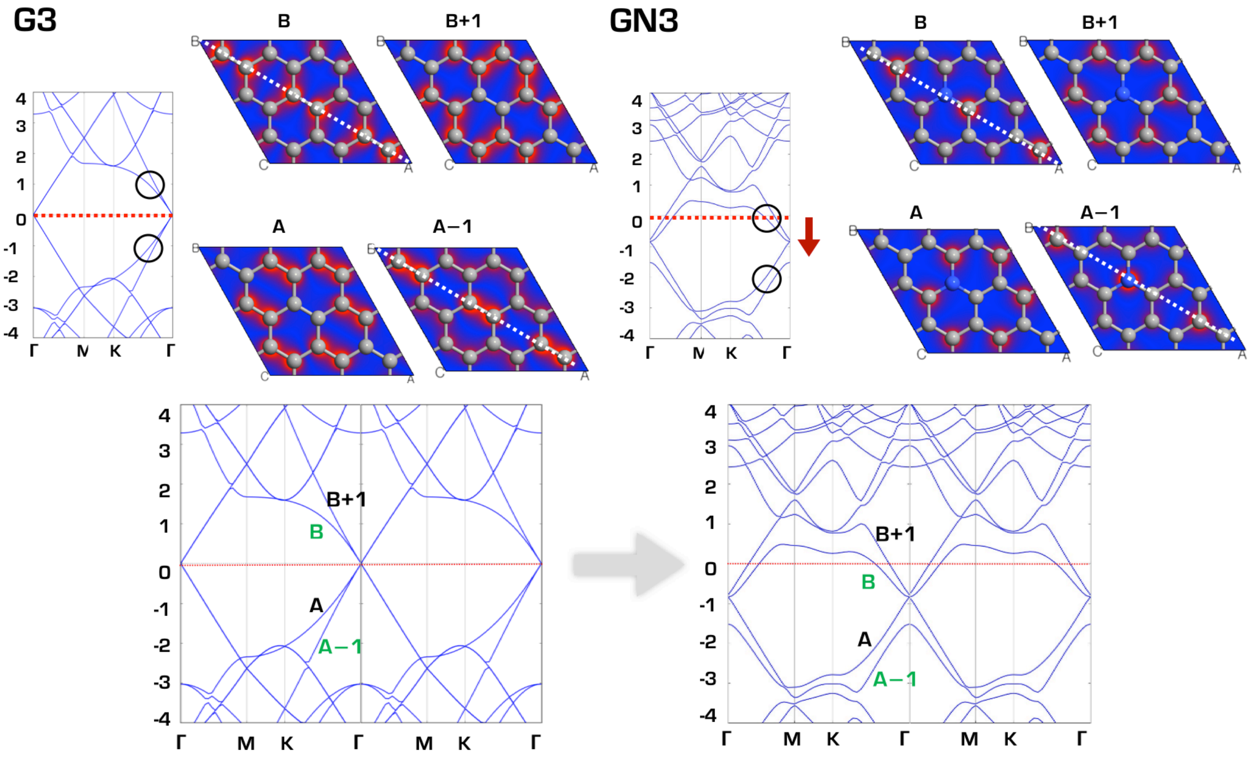

Figure S3. Bloch states near the Γ point of G3 and GN3 and band distortion due to introduction of n-type nitrogen dopant. B and B+1, and A and A−1 are degenerated conducting and valence bands at Dirac point.

The pristine G3 shows two linear band pairs of similar Bloch states (B+1/A and B/A−1 pairs), which reaches the same point at Fermi level leading to zero gap. In contrast, the band structure of GN3 gives overall downshift of band due to n-type doping of nitrogen and one split band pair because dopant predominantly affects B and A−1 Bloch states. Therefore, the B and A−1 band pair shows a curved shape with a large band gap.

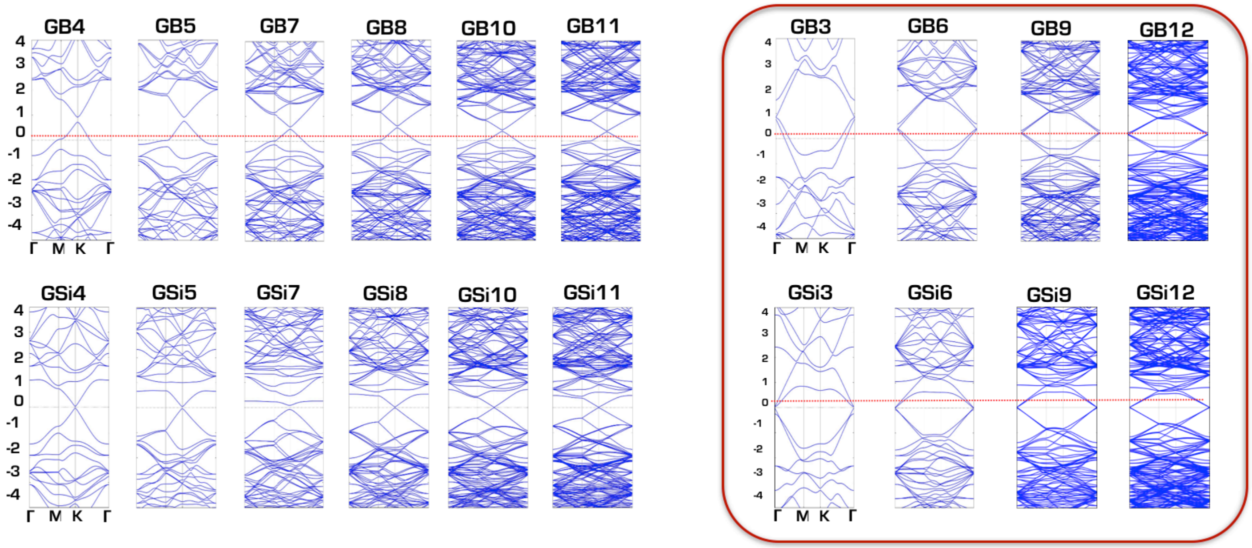

Figure S4. Band structures of GB and GSi with *N* x *N* primitive cell sizes.

Table S1. Zero point energies (ZPE) and entropic (TS) corrections for heteroatom doped-graphenes (G, GB, GN, GP, GS, and GSi) at 298 K.

eV	ZPE	TS	△ZPE	T△S	△ZPE- T△S
G-H*	0.25	-	0.11	-0.210	0.32
GB-H*	0.25	-	0.12	-0.210	0.32
GN-H*	0.29	-	0.16	-0.210	0.36
GP-H*	0.30	-	0.17	-0.210	0.37
GS-H*	0.31	-	0.18	-0.210	0.38
GSi-H*	0.30	-	0.17	-0.210	0.37
H_2	0.27	0.41	-	-	-

The gas phase values were from Ref. 1, while the values for the adsorbed species were taken from DFT calculations. The same values for the adsorbed species for all the *N X N* models were used, as vibrational frequencies have been found to depend much less on the surface than the bond strength.

$$\frac{1}{2}H_2 + * \rightarrow \frac{1}{2}H_2^*$$

$$\Delta ZPE = ZPE_{\frac{1}{2}H_2^*} - \frac{1}{2}ZPE_{H_2}$$

$$\Delta S = S_{\frac{1}{2}H_2^*}(\approx 0) - \frac{1}{2}S_{H_2}$$

Table S2. Frequencies of adsorbed species of heteroatom doped-graphenes (G, GB, GN, GP, GS, and GSi)

Adsorbed Species	Frequency (cm^{-1})
G-H*	822.150, 871.508, 2297.860
GB-H*	633.542, 990.878, 2474.089
GN-H*	1097.330, 1262.868, 2307.007
GP-H*	992.801, 1131.792, 2773.806
GS-H*	1090.338, 1129.199, 2813.658
GSi-H*	844.864, 1142.589, 2870.745

Reference

1. P. W. Atkins, Physical Chemistry, sixth ed., Oxford University Press, Oxford (1998).

Table S3. The calculated adsorption energies of hydrogen atoms in subsequent Volmer step considering possible binding sites around the dopant at 6 X 6 supercell.

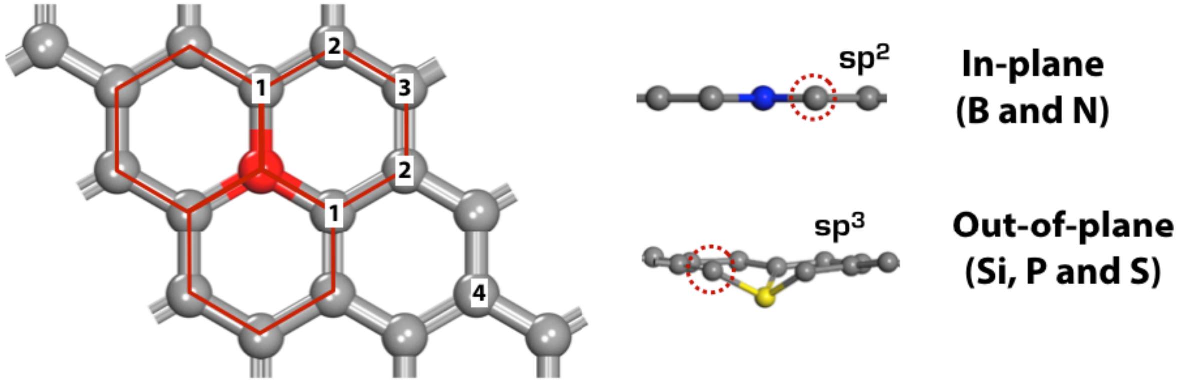

$^{a}E_{b1}$ (eV)	Site1	Site2	Site3	Site4
GN6	**0.36**	0.77	0.53	0.94
GS6	**-0.29**	0.85	0.62	1.31
$^{b}E_{b2}$ (eV)	Site1-1	Site1-2	Site1-3	Site1-4
GN6	0.50	**0.43**	0.87	1.02
GS6	**0.02**	0.28	0.74	1.18
$^{c}E_{bt}$ (eV)	Site1-1	Site1-2	Site1-3	Site1-4
GN6	0.86	**0.78**	1.23	1.38
GS6	**-0.27**	0.00	0.45	0.89

$^{a}E_{b1} = E(GX + H) - [E(GX) + \frac{1}{2}E(H_2)]$

$^{b}E_{b2} = E(GX + 2H) - [E(GX + H) + \frac{1}{2}E(H_2)]$

$^{c}E_{b1} = E(GX + 2H) - [E(GX) + E(H_2)]$

Our calculations show that the first hydrogen atom favorably bind to **site1** in both in-plane (GN) and out-of-plane (GS) structure with 0.36 eV and -0.29 eV, respectively. But, the second hydrogen atom in the in-plane and out-of-plane structures prefers **site2** and **site1** with 0.43 eV and 0.02 eV, respectively. The results are well agreement with our interpretation based on the atomic orbital hybridization analysis described in the main text, where the subsequent two hydrogen atoms prefer to bind to only sp^3 hybridized carbons adjacent to the dopant in out-of-plane structures, and in the in-plane structures, the second hydrogen atom favorably bind to sp^3 hybridized second neighboring carbons of dopant. In out-of-plane structures, the subsequent two hydrogen atoms prefer to bind to only sp^3 hybridized **site1** carbons. However, in the case of in-plane structures having only sp^2 hybridized carbons, the first hydrogen atom should result in structural deformation to form sp^3 hybridized carbons. Therefore, the first hydrogen adsorption on the in-plane structure is less favorable than the reaction on out-of-plane structures. And the second hydrogen atom can favorably bind to sp^3 hybridized **site2** carbons.